Biol. Cell (2017) **109,** 1–19 DOI: 10.1111/boc.201600082

Research article

Exposure to *Bordetella pertussis* adenylate cyclase toxin affects integrin-mediated adhesion and mechanics in alveolar epithelial cells

Christelle Angely*†‡[2], Ngoc-Minh Nguyen*†‡[2], Sofia Andre Dias*†‡, Emmanuelle Planus§, Gabriel Pelle*†‡‖, Bruno Louis*†‡, Marcel Filoche*†‡#, Alexandre Chenal, Daniel Ladant** and Daniel Isabey*†‡[1]**

*Inserm, U955, Equipe 13, Biomécanique & Appareil Respiratoire: une approche multi-échelle, Créteil Cedex 94010, France, †Université Paris Est, UMRS 955, UPEC, Créteil Cedex 94010, France, ‡CNRS, ERL 7240, Créteil Cedex 94010, France, §Institute for Advanced Biosciences (IAB), Centre de Recherche UGA/Inserm U1209/CNRS UMR 5309, La Tronche 38700, France, ‖AP-HP, Groupe Hospitalier H. Mondor - A. Chenevier, Service des Explorations Fonctionnelles, Créteil Cedex 94010, France, #Laboratoire de Physique de la Matière Condensée, Ecole Polytechnique, CNRS, Université Paris Saclay, Palaiseau 91128, France, and **Unité de Biochimie des Interactions Macromoléculaires (CNRS UMR 3528), Département de Biologie Structurale et Chimie, Institut Pasteur, Paris 75014, France

Background Information. The adenylate cyclase (CyaA) toxin is a major virulent factor of *Bordetella pertussis*, the causative agent of whooping cough. CyaA toxin is able to invade eukaryotic cells where it produces high levels of cyclic adenosine monophosphate (cAMP) affecting cellular physiology. Whether CyaA toxin can modulate cell matrix adhesion and mechanics of infected cells remains largely unknown.

Results. In this study, we use a recently proposed multiple bond force spectroscopy (MFS) with an atomic force microscope to assess the early phase of cell adhesion (maximal detachment and local rupture forces) and cell rigidity (Young's modulus) in alveolar epithelial cells (A549) for toxin exposure $<$1 h. At 30 min of exposure, CyaA toxin has a minimal effect on cell viability ($>$95%) at CyaA concentration of 0.5 nM, but a significant effect ($\approx$81%) at 10 nM. MFS performed on A549 for three different concentrations (0.5, 5 and 10 nM) demonstrates that CyaA toxin significantly affects both cell adhesion (detachment forces are decreased) and cell mechanics (Young's modulus is increased). CyaA toxin (at 0.5 nM) assessed at three indentation/retraction speeds (2, 5 and 10 μm/s) significantly affects global detachment forces, local rupture events and Young modulus compared with control conditions, while an enzymatically inactive variant CyaAE5 has no effect. These results reveal the loading rate dependence of the multiple bonds newly formed between the cell and integrin-specific coated probe as well as the individual bond kinetics which are only slightly affected by the patho-physiological dose of CyaA toxin. Finally, theory of multiple bond force rupture enables us to deduce the bond number N which is reduced by a factor of 2 upon CyaA exposure ($N \approx 6$ versus $N \approx 12$ in control conditions).

Conclusions. MFS measurements demonstrate that adhesion and mechanical properties of A549 are deeply affected by exposure to the CyaA toxin but not to an enzymatically inactive variant. This indicates that the alteration of cell mechanics triggered by CyaA is a consequence of the increase in intracellular cAMP in these target cells.

Significance. These results suggest that mechanical and adhesion properties of the cells appear as pertinent markers of cytotoxicity of CyaA toxin.

Additional supporting information may be found in the online version of this article at the publisher's web-site

[1]To whom correspondence should be addressed (email: daniel.isabey@inserm.fr)
[2]These authors contributed equally to this work.
Key words: Adenylate cyclase, Adhesion, Cellular stiffness, Rupture force, Toxin.

Abbreviations: AECs, alveolar epithelial cells; AFM, atomic force microscopy; CyaA, adenylate cyclase; cAMP, cyclic adenosine monophosphate; FS, force spectroscopy; MFS, multiple bond force spectroscopy; RT, room temperature.

Introduction

The adenylate cyclase (CyaA) toxin is one of the main virulent factors of the bacteria *Bordetella pertussis* (Bp) – the whooping cough agent (Khelef et al., 1992; Ladant and Ullmann, 1999; Carbonetti, 2010). CyaA toxin possesses the remarkable property of translocating its catalytic domain into the cytosol of eukaryotic cells where it is activated by an endogenous protein, calmodulin to produce supra-physiological levels of cyclic adenosine monophosphate (cAMP) which in turn alter cell physiology (Ladant and Ullmann, 1999; Vojtova et al., 2006; Carbonetti, 2010). The process by which the catalytic domain is translocated across the plasma membrane is called internalisation or intoxication (Ladant and Ullmann, 1999). There are several experimental evidences supporting that internalisation occurs through a direct translocation of CyaA catalytic domain across the plasma membrane of target cells (Veneziano et al., 2013). First, increased levels of cAMP can be detected within seconds after adding CyaA toxin (by contrast, entry of toxins through endocytosis and vesicular trafficking would require a much longer exposure time). Accordingly, CyaA toxin plays a key role in the early stages of respiratory tract colonisation. Second, its entry is independent of both acidification of endocytic vesicles and cytochalasin D treatment (Mouallem et al., 1990), an inhibitor of F-actin polymerisation which affects actin-related functions (Qualmann et al., 2000). Although the exact process of toxin internalisation is not fully understood, it is considered to be a two-step process implicating: (1) binding to the cell surface through interaction with integrin receptor CD11b/CD18 (or $\alpha_M\beta_2$) (Guermonprez et al., 2001) or through direct contact with the lipid membrane (Gray et al., 2004), and (2) translocation of the catalytic domain in which CyaA might use the electrical field across the plasma membrane as a driving force to enter target cells (Otero et al., 1995; Veneziano et al., 2013).

CyaA toxin plays a key role in the early stages of respiratory tract colonisation (Vojtova et al., 2006; Carbonetti, 2010). To disable the innate immune responses, CyaA toxin targets immune cells such as macrophages and neutrophils that express the main toxin receptor, the β_2-integrin receptor CD11b/CD18 (or $\alpha_M\beta_2$) (Guermonprez et al., 2001) and rapidly increases the intracellular cAMP concentration. In macrophages, inactivation of the GTPase RhoA by CyaA toxin leads to actin cytoskeleton rearrangements including membrane ruffling and alterations of phagocytic functions (Kamanova et al., 2008). In addition, CyaA can induce apoptosis associated with caspase activation and thus promote the activation of cell death cascade in macrophages cells (Gueirard et al., 1998; Ahmad et al., 2016). However, CyaA toxin also invades a broad range of cells that do not express CD11b/CD18, although the functional and patho-physiological consequences of CyaA cytotoxicity are not fully understood. In particular, CyaA toxin is able to invade the epithelial cells of the conductive respiratory tract (Eby et al., 2010). In cultured epithelial cells free of the $\alpha_M\beta_2$ receptor, CyaA causes cell rounding (Ohnishi et al., 2008). Besides, CyaA toxin is assumed to induce apoptosis associated with caspase activation in a variety of cells including lung cancer cell lines (Carbonetti, 2010). To our knowledge, the cytotoxic effect of CyaA toxin in alveolar epithelial cells (AECs) remains not documented.

AECs can also be directly exposed to bacterial invasion when the airway defence system is depleted, for example secondary to the impairment of mucociliary transport caused by particular patho-physiological conditions (chronic obstructive pulmonary disease and asthma) and/or specific genetic abnormalities. Even when structural cilia defects are not identified, cilia function can still be impaired by various exposures to toxins. These toxins can affect cilia function directly or can modify the secretions and viscosity of the mucus layer which is transported by the mucociliary escalator (Yaghi and Dolovich, 2016). Whether CyaA invasion is able to modify the distal respiratory alveolar epithelium during *B. pertussis* colonisation remains presently unknown.

In the present study, we explore the mechanical and adhesion properties of AECs (A549 cell line) to quantify the short term response to CyaA cytotoxicity at the cellular and molecular levels. We used atomic force microscopy (AFM) and an improved analysis of cell–matrix adhesion named multiple bond force spectroscopy (MFS) described in a companion paper (Nguyen et al., 2017). The model-system used in the present study is a culture of A549 cells exposed to various concentrations of CyaA toxin. Three values of CyaA concentration are tested (0.5, 5 and 10 nM) which is a range covering, for the lowest dose tested, the patho-physiological conditions (*i.e.* up to

100 ng/ml – about 0.6 nM – at the bacterial cell interface according to Eby et al., 2013) and for the two higher dose tested the supra-physiological conditions already used to compensate the lack of $\alpha_M\beta_2$ integrin receptors in presently tested A549 cells. Here, we explore whether this range of CyaA concentration affects the adhesion and mechanical properties (*i.e.* cell rigidity – Young's modulus – and in cell adhesion strength – detachment and rupture forces) of AECs (A549) using MFS and AFM. The MFS results along with cell imaging provide consistent experimental evidences that CyaA toxin has a significant role on cytoskeleton and adhesion structures from the smallest dose of CyaA toxin tested, that is 0.5 nM, not only in terms of number of associated bonds but also in terms of energy of individual integrin–ligand bonds. Present results suggest that mechanical and adhesive properties appear as pertinent markers of the cytotoxic effect of CyaA in non-inflammatory cells.

Results

Viability of cells exposed to CyaA toxin

We first demonstrate that in human AECs (A549) exposed to CyaA toxin for times between 15 and 60 min, a significant dose-dependent increase in cAMP (order(s) of magnitude higher than control) is observed for the three tested CyaA concentrations, while a CyaA variant lacking enzymatic activity, CyaAE5, has no effect on intracellular cAMP levels (Figure 1A).

Second, viability of A549 human AECs is measured for different durations (15, 30 and 60 min) and for different concentrations of the CyaA toxin (Figure 1B). These results are compared with the viability of cells exposed to an enzymatically inactive variant of CyaA, CyaAE5 (Figure 1C). We find a dose-dependent decrease in cell viability for cells exposed to the active CyaA toxin but a wide majority of cells remain viable because of the limited duration of MFS experiments. The CyaA toxin effect on cell viability becomes significant only at the highest concentration tested (10 nM). By contrast, CyaAE5 does not modify the cell viability at all concentration or exposure duration tested. Most importantly, exposure of the A549 cells to the lowest concentration (0.5 nM) of CyaA toxin within limited periods of time (30 min on the average in present MFS experiments), leads to negligible cell death (viability >95%) and in any case to non-significant differences with control conditions. For supra-physiological concentrations of CyaA, cell viability at 30 min of CyaA exposure decreases to 87%-viability at 5 nM and 81%-viability at 10 nM. Based on these results, accurate quantifications of adhesion in exposed cells are performed for CyaA concentrations for which a maximum number of cells remain alive.

CyaA effects on F-actin and focal adhesion structures

Figure 2 shows fluorescent images of F-actin network (Figure 2D), focal adhesions (Figure 2E) and merge (Figure 2F), in A549 cells exposed to CyaA toxin for 30 min of duration at a low concentration of 0.5 nM (at which a maximum number of cells remain alive) by comparison with control conditions (Figures 2A–2C, respectively). Quantifications of fluorescent F-actin and number of focal adhesion points are presented in Figures 2G and 2H. We find significant differences in F-actin level and average number of adhesion points between cells exposed to CyaA toxin and the control group. By comparison with the cells exposed to the lowest concentration tested (Figure 2), the two highest CyaA concentrations tested (5 and 10 nM) (see Supplementary Figure 4) induce marked concentration-dependent alteration on F-actin structure with disappearance of stress fibres (see arrows in Supplementary Figure 4A, D and bar graphs in Supplementary Figure 4G) and loss in focal adhesion points (see dotted arrows in Supplementary Figure 4B, E and bar graphs in Supplementary Figure 4H). Confocal images of the fluorescent F-actin structures (Figure 2 and Supplementary Figure 4) obtained at 30 min exposure show that this concentration-dependent remodelling of the cytoskeleton and adhesion points results in a significant increase in cell height (see Supplementary Figure 2).

CyaA effect on cell adhesion and cell mechanics assessed by MFS

MFS is performed on top of living adherent cells (only one force–distance curve performed per cell) whose viability is assessed cell-by-cell by their characteristic shape evaluated on transmission images (and not by the Trypan test that was used only for data showed in Figures 1B and 1C – see Material and Methods and Supplementary Figure 1). Exposure to increasing concentrations of CyaA toxin deeply modified

Figure 1 | **See Legend on next page**

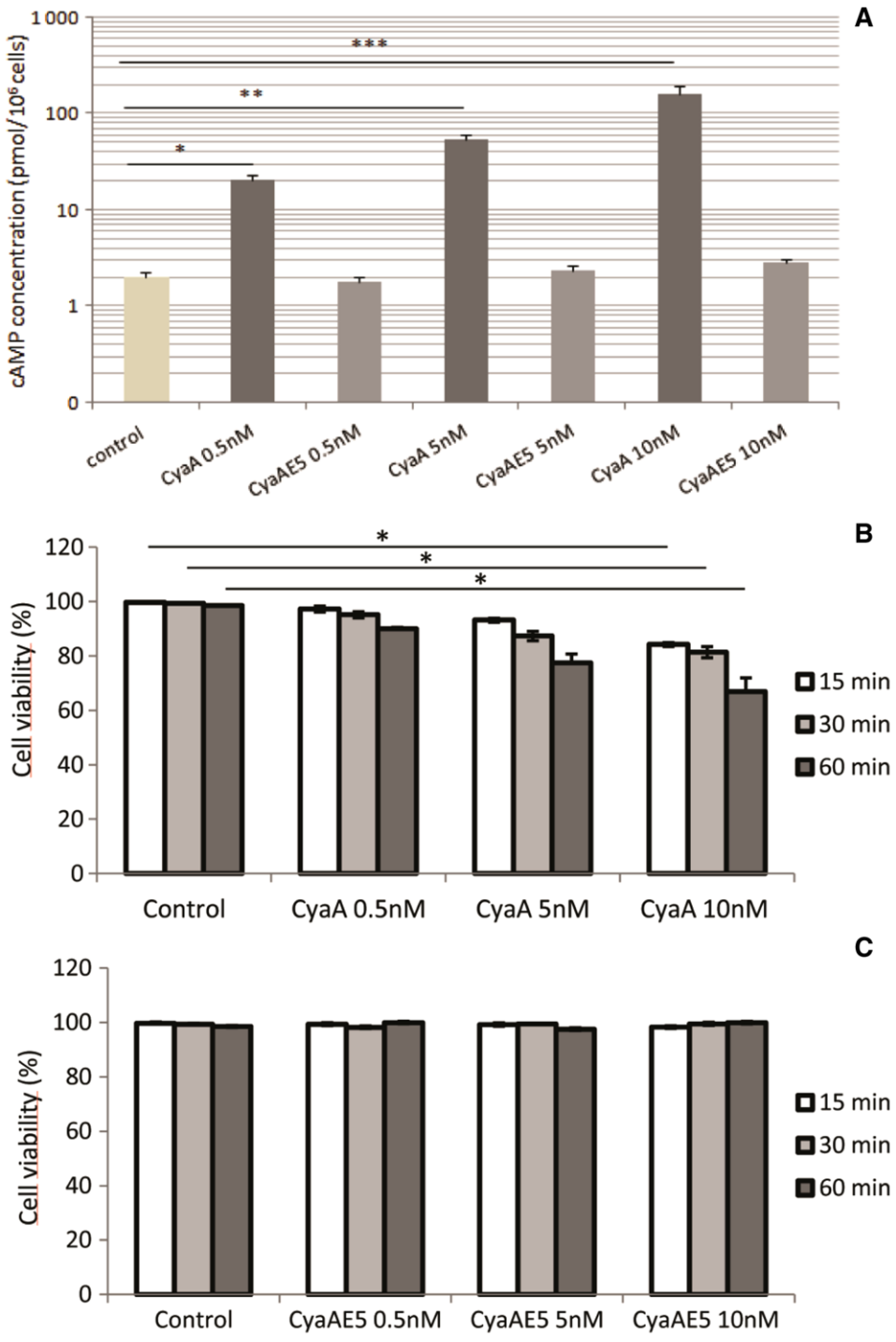

Figure 1 | Intracellular cAMP measurement and viability tests performed on A549 cells

Intracellular cAMP measurement (**A**) and viability test (**B** and **C**) performed on A549 cells for control conditions, and cells exposed to active (**B**) and enzymatically inactive variant of CyaA, CyaAE5 (**C**). Cell viability is measured as percentage of living cells after 15, 30 or 60 min of exposure. (**A**) The cAMP intracellular concentrations in A549 cells for control conditions ($n = 6$) or after exposure to the indicated concentrations of CyaA ($n = 6$) for times corresponding to MFS experiment duration (15–60 min), or the enzymatically inactive variant CyaAE5 ($n = 6$), were determined by an ELISA assay (see *Materials and Methods*). This bar graph shows that the intracellular concentration of cAMP in cells exposed to CyaA toxin increases significantly with the increase in the concentration of CyaA toxin, while CyaAE5 has no detectable effect on cAMP as expected. (**B**) From left to right, control conditions (complete medium with the toxin dilution buffer) ($n = 6$), and CyaA concentrated at 0.5, 5 and 10 nM ($n = 6$). (**C**) From left to right, control conditions (complete medium with the toxin dilution buffer) ($n = 6$), and CyaAE5, concentrated at 0.5, 5 and 10 nM ($n = 6$). The effect of CyaA on cell viability is dose dependent and not really time dependent. The cell viability decreases with increasing CyaA concentration up to significance at 10 nM ($p \leq 0.05$) but the time of exposure has a negligible effect within a maximal experimental duration of 60 min. Error bars are ±SEM $^{*}p \leq 0.05$; $^{**}p \leq 0.01$; $^{***}p \leq 0.001$.

the recorded force–distance curves, especially because at the highest concentrations where some detached cells (see Supplementary Figure 1) are susceptible to generate a perturbation in the cantilever motion, as shown in Supplementary Figure 3 with 10 nM CyaA. Before studying CyaA toxin effects on cell adhesion and mechanics, we verified in control experiments that: (i) the RGD coating was stable throughout the time of AFM experiments by changes in the maximal detachment force. These changes considered at different times and for different retraction speeds remained limited to the intercellular variability and not significant (see Supplementary Figure 5A), (ii) the probe coating was specific by comparing the values of maximal detachment forces for specific and non-specific coating conditions and verifying that the RGD-coating condition leads to the highest adhesion forces (see Supplementary Figure 5B), and that (iii) the CyaA dilution buffer used to CyaA condition (see Material and Methods) had no effect on the measured cellular parameters if CyaA toxin is not present (results not shown).

The effects of various concentrations of CyaA toxin (0.5, 5 or 10 nM) are studied (at v = 5 μm/s) on AECs for exposed to the toxin for less than 60 min maximum (30 min on the average). Results are presented in Figure 3 and in Supplementary Table 1. Each point corresponds to a different cell. Cell exposure to CyaA toxin results in significant effects on cell adhesion: the maximal detachment force $F^*$and the work of adhesion W_{adh} are significantly decreased compared with control conditions suggesting adhesion weakening at the apical cell surface in presence of CyaA toxin. By comparison, the enzymatically inactive variant of CyaA, CyaAE5, had no effect.

Interestingly, the effect of CyaA on Young modulus appears more significant at the lowest CyaA concentration (0.5 nM) as no significant change in E_{cell} was observed at 5 nM CyaA. This might be due to some compensatory effects occurring for intermediate levels of CyaA concentration, the reinforced alteration in actin structure counterbalancing the mechanical effects observed at the lower dose of CyaA toxin. The large variations in mechanical properties shown in Figure 3C provide an idea of the mechanical variability which could in turns affect the variability in loading rate though Eq. (6) (Supplementary Table 2) and beyond the variability in F^*through Eq. (5) (Figure 3A and Supplementary Table 2).

Global effects of CyaA at different indentation/retraction speeds

In order to assess the role of the loading rate on measured cellular parameters F^*, W_{adh} and E_{cell}, we first need to extend the range of loading rates by testing various indentation–retraction speeds. To do so, we only used the CyaA concentration (0.5 nM), and compare the results for the three different retraction speeds (v = 2, 5 and 10 μm/s) (see Figure 4 and also values in Supplementary Table 2). Depending on the speed tested, CyaA exposure leads to significant differences (compared with control conditions) for maximal detachment force F^*, work of adhesion W_{adh} and Young modulus E_{cell}. The cellular effects observed at the three speeds appear consistent: adhesion parameters $F^*$and W_{adh} are decreased meaning that newly formed adhesion is weakened, and Young modulus parameter E_{cell} is increased meaning that CyaA toxin tends to stiffen the cells. The

Figure 2 | Cell imaging for F-actin structure and focal adhesion points

Co-staining of F actin (phalloidin, in red) and of focal adhesion (phosphotyrosin PY99, in green) in fixed A549 cells after 30 min of exposure to control conditions or CyaA toxin. (**A and D**) F-actin staining, (**B and E**) focal adhesion staining, (**C and F**) merge. (**A–C**) Control conditions ($n = 13$), (**D–F**) cell exposure to CyaA concentrated at 0.5 nM cells ($n = 13$). (**G**) Quantification of F-actin fluorescence for control conditions and after exposure to CyaA concentrated at 0.5 nM. (**H**) Average number of focal adhesions per cell, control conditions and CyaA exposure. F-actin in control conditions is reticulated and exhibits a highly organised stress fibres network (white arrows in A). After CyaA exposure, F-actin structure is weakened which is confirmed by the significant decay ($p \leq 0.05$) in fluorescent F-actin between control conditions and CyaA-exposed cells (number of white arrows is decreased in **D**). Control cells also have numerous focal adhesions (white dotted arrows in **B**) linked to actin stress fibres near the cell periphery (grey arrows in **C**) and a smaller number around the cell centre. After CyaA exposure, focal adhesions at the periphery of the cell are less intense than in control (number of dotted and grey arrows is decreased in **E** and , respectively). There is a significant decay in the number of focal adhesions per cell after CyaA exposure (in H) ($p \leq 0.05$). Scale bar represents 20 μm. Error bars are $\pm$SEM. $^{*}p \leq 0.05$; $^{**}p \leq 0.01$; $^{***}p \leq 0.001$.

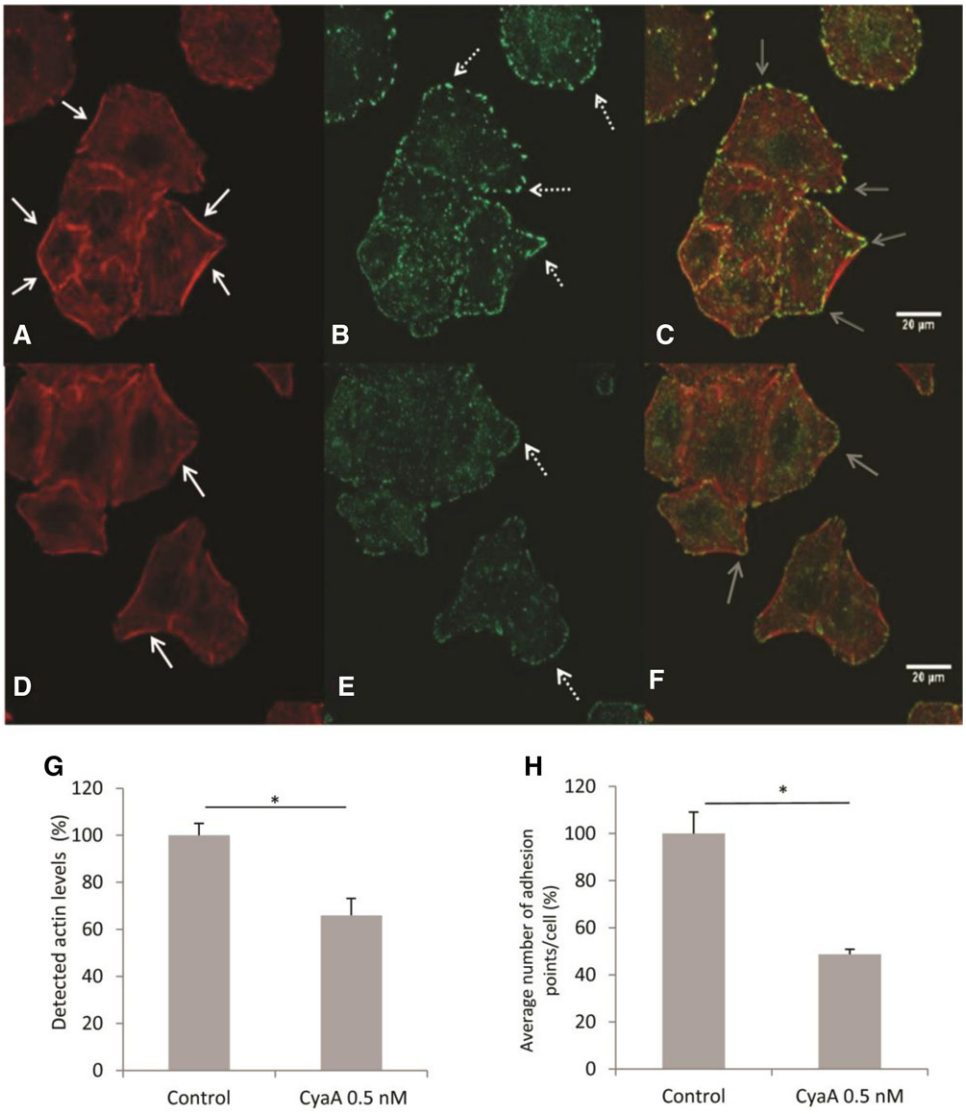

Figure 3 |

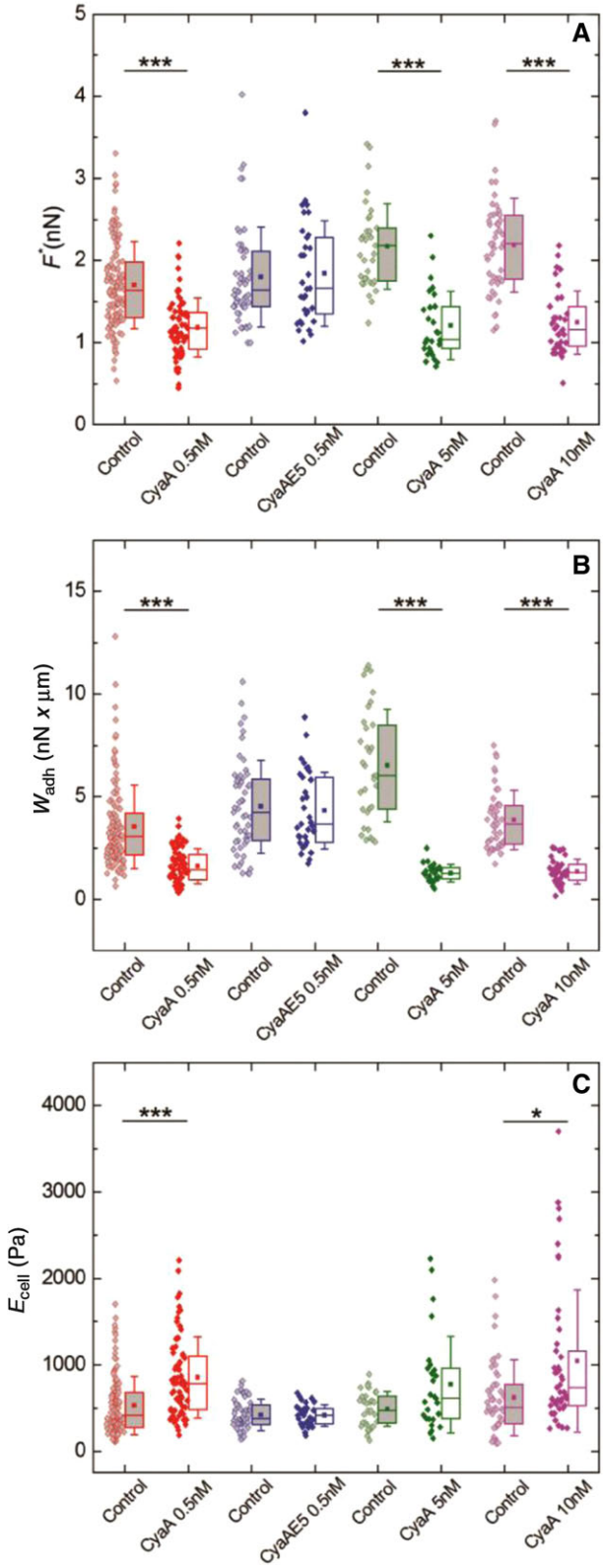

Figure 3 | MFS results in A549 cells exposed to various concentrations of CyaA toxin

(**A**) The maximal detachment force F^* (in nN), (**B**) the work of adhesion W_{adh} (in nN $\times$ μm) and (**C**) the Young's modulus E_{cell} (in Pa) measured during MFS experiments. Each data point on A, B, C, corresponds to a different cell. Indentation and retraction speeds are fixed at $v = 5$ μm/s. Data are obtained in A549 cells for control condition, exposure to three concentrations of CyaA toxin (0.5, 5 and 10 nM) and one concentration (0.5 nM) of CyaAE5 toxin. Compared with each control condition: F^* and W_{adh}, are significantly decreased for the three CyaA concentration tested ($p < 0.001$). In the case of CyaAE5, there is no difference with the control condition. For E_{cell}, there is significant differences between control and exposure to CyaA toxin at the lowest CyaA concentration (0.5 nM) ($p < 0.001$) and the highest (10 nM) ($p < 0.05$) but no significant differences at 5 nM. The squares in rectangular boxes mark the mean value, whisker bars the $\pm$SD values, and the horizontal line in each box gives the median value. $^*p \leq 0.05$; $^{**}p \leq 0.01$; $^{***}p \leq 0.001$. Number of tested cells is detailed in Supplementary Table 1. The lack of dose-dependent consistency in the cell mechanical behaviour seems associated to a larger intercellular variability associated to CyaA exposure.

large dispersion of data which is associated to the intercellular variability renders difficult the observation of a significant speed-dependent effect on measured parameters, hence the need to consider the cell-by-cell values of cell stiffness and beyond its effect on the actual value of loading rate, proper to each cell.

The effect of CyaA on adhesion and mechanical parameter dependence of loading rate

The use of three retraction speeds in the range 2–10 μm/s has permitted to extend over about 2 decades the range of global loading rates (Figure 5). The loading rate is calculated cell-by-cell using Eq. (7). The cellular stiffness k_{cell} which enters in the calculation of the global loading rate r_f is deduced from: $k_{cell} = E_{cell} \times \delta$ where the characteristic distance δ is estimated cell-by-cell from the ratio: $\delta = W_{adh}/F^*$ (see in Supplementary Table 2 the mean $\pm$SD values of E_{cell}, δ and r_f obtained on each tested cell populations (n) at CyaA concentration of 0.5 nM). To characterize the relationships between F^* and the global loading rate r_f, two methods of data analysis are used and results are presented in Figure 5 and upper part of Table 1: (i) a linear regression performed

Figure 4 |

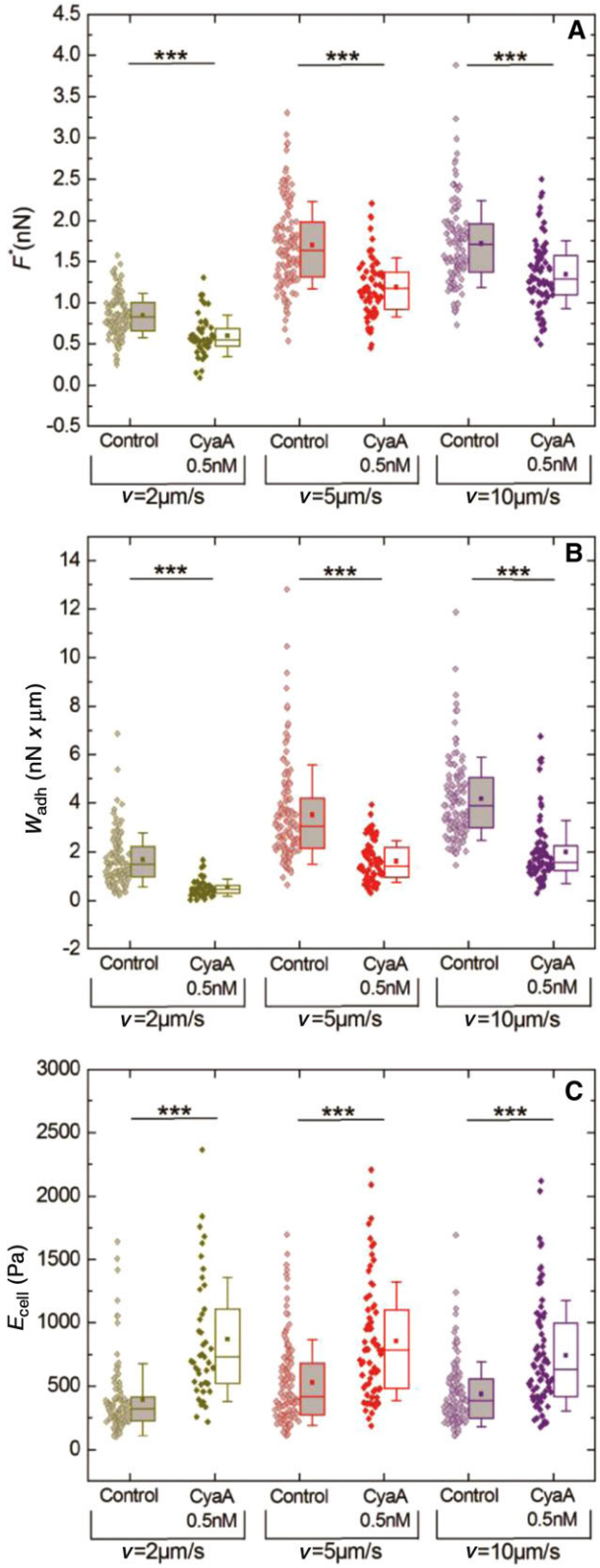

Figure 4 | MFS results for global parameters in CyaA-exposed A549 cells, obtained at various indentation/retraction speeds

(**A**) The maximal detachment force F^* (in nN), (**B**) the work of adhesion W_{adh} (in nN $\times$ μm) and (**C**) the Young's modulus E_{cell} (in Pa) measured during MFS experiments and three different predetermined indentation/retraction speeds: $v = 2$, 5 and 10 μm/s. Each data point on A, B, C, corresponds to a different cell. Data are obtained in A549 cells for control condition, and exposure to the lowest concentrations of CyaA toxin (0.5 nM). Compared with their respective control condition, F^* and W_{adh}, are significantly decreased for the three tested speeds ($p < 0.001$). For E_{cell}, there is a systematic significant increase ($p < 0.001$) compared with the respective control condition. The squares in rectangular boxes mark the mean value, whisker bars the $\pm$SD values, and the horizontal line in each box gives the median value. $^*p \leq 0.05$; $^{**}p \leq 0.01$; $^{***}p \leq 0.001$. Number of tested cells is detailed in Supplementary Table 2.

on all data points obtained at the three tested speeds, each point representing a different cell (see the continuous line in Figure 5), (ii) a linear regression performed on the three mean $\pm$ SD values of F^* and obtained at each one of the three retraction speeds tested (v = 2, 5 and 10 μm/s). The first method (large number method) is based on the law of large numbers which states that because of large number of data points, the found relationship is close to the expected relationship predicted by the probability theory for multiple bond rupture (Eq. (5)). The second method (three-point method) tends to mimic the classical approach in which a statistically meaningful value of F^* depends on a statistically representative value of r_f (see values in Table 1). The graph of F^*versus ln r_f obtained on a wide number of cells leads to a linear regression analysis ($R = 0.6$) which is a rather low value due to intercellular variability). The slope of this relationship gives F_β and the intercept at $r_f = 1$ pN/s enables to estimate K^0_{off} from the vertical intercept. Practically, the large number method leads to $F_\beta = 280$ pN and $K^0_{off} = 0.28\ s^{-1}$, while the three-point method ($R = 0.99$) leads to $F_\beta = 379$ pN and $K^0_{off} = 0.73\ s^{-1}$. Because the energy landscape of the multiple bond is highly complex, it is difficult to conclude about the CyaA effect at the global level without considering the energetic

Figure 5 | Force–loading rate relationship at the global cellular level

The relationship between the maximal detachment force $F*$(in pN) and the global loading rate r_f (in pN/s) plotted on a logarithmic scale for CyaA toxin at the smallest concentration (0.5 nM) and for the three predetermined speeds: $v = 2$ μm/s (green points), $v = 5$ μm/s (red points) and $v = 10$ μm/s (purple points). The slope of the linear regression (continuous line) give the reference force F_β and the intercept with vertical axis at $r_f = 1$ pN/s enables to calculate the natural dissociation rate K^0_{off} (in s^{-1}) from the relation $[F^*]_{\ln r_f=0} = -f_\beta \ln(K^0_{off} F_\beta)$. Note that each data point represents a different cell. The dotted line represents the linear regression obtained for control condition (data points of control condition are not plotted on this graph).

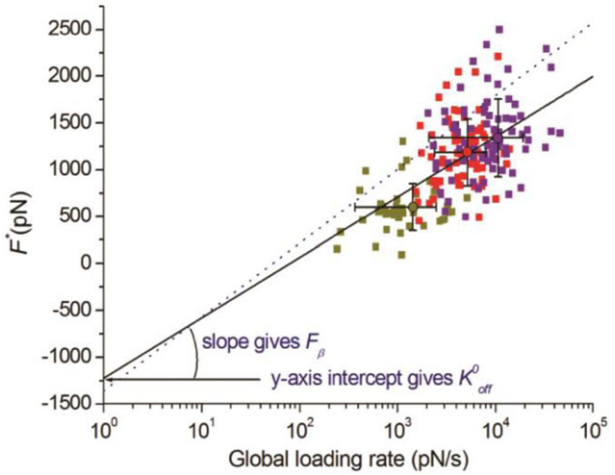

characteristics of the individual rupture events. This is done below.

Local effects of CyaA at different indentation/retraction speeds

The effect of CyaA toxin (0.5 nM) on individual bonds can be characterised by the statistics of the local rupture force f^* obtained at the three different speeds tested. f^* values characterize the local rupture events observed on the force–distances curves already used to analyse the effect of CyaA toxin on global parameters. There are several rupture events appearing on each force–distance curve but the number of rupture event is susceptible to be affected by the exposure to CyaA toxin at 0.5 nM. Results presented in Figure 6A reveal that, during CyaA exposure, f^* is significantly higher than control values. Note however that dispersion of data remains important likely due to the intercellular and molecular variability in the biological and mechanical cell properties. Histograms of local rupture forces for the different speeds tested (Figure 6B) show that the values of f^*roughly follow a Gaussian distribution except at the highest speed tested. Nevertheless, the closeness between the median values and the mean values systematically observed at the three tested speeds (Figure 6A) confirms that the values of f^* remain close to a Gaussian (or normal) distribution. The effect of CyaA exposure on local rupture forces differs from the one observed at the global scale. One possible reason is that the local stiffness (and thus the local loading rate) measured during CyaA exposure is sensibly higher compared with that of control conditions (Supplementary Table 2). The analysis of local rupture events must therefore be directly performed as a function of the local loading rate.

The effect of CyaA on the local loading rate dependence of local cellular parameters

Individual rupture events can be characterised by the relationships between rupture force f^* and local loading rates r_f obtained from the slope on the final part of the retract force–displacement curve preceding the point of bond rupture (see *Material and Method* and insert in Figure 8B). However, because the force rupture analysis requires an estimate of the loading rate, only values of rupture events preceded by a negative slope (local stiffness) are analysed in the graph of Figure 7. As for global data, we used the large number method and the three-point method to analyse the local rupture events. Using the large number method, the relationship between f^* and $\ln r_f$ can be adequately fitted by a linear regression ($R = 0.77$) (continuous line shown in Figure 7) whose slope provides $f_\beta = 45$ pN and the intercept at $r_f = 1$ pN/s provides an estimate of $k^0_{off} = 1.02\ s^{-1}$ (Table 1). Using the three-point method, the linear regression ($R = 0.99$) leads to $f_\beta = 61$ pN and $k^0_{off} = 1.94\ s^{-1}$ showing that the two methods lead to consistent estimates. By comparison with the adhesion parameters obtained in control conditions (see dotted line in Figure 7), the present evolutions of f_β and k^0_{off} caused by CyaA toxin (see Table 1) suggest that the height of the energy barrier of the integrin–ligand is only

Table 1 | The Adhesion Parameters Obtained from the Linear Regressions Analysis at Global and Local Levels
Characterisation of the relationships force–loading rate obtained globally at the cell scale and locally for each rupture event for CyaA toxin condition at 0.5 nM compared with control condition (values noted in parenthesis correspond to the dotted lines in Figures 6 and 8). For the three first columns: values correspond to the slope and intercept parameters of the linear regression done on either the whole data set (continuous lines in Figures 6 and 8) or the three points obtained by averaging of data corresponding to each constant speed. For the three last columns, adhesion parameters are deduced from the linear regression analysis. In control conditions, there are 332 force–curves (*i.e.* cells) analysed for global rupture events and 171 (≈50%) interpretable rupture events leading to the determination of the parameter values (in parenthesis) issued from the force–loading rate analysis. By contrast, with CyaA at 0.5 nM concentration, there are 187 force–curves (*i.e.* cells) analysed for global rupture events and only 50 (≈27%) interpretable events, leading to the determination of the parameter values issued from the force–loading rate analysis presented in Figure 7.

		Vaues for exposure to CyaA 0.5 nM					
		Slope $\approx F_\beta$(pN)	Intercept (pN)	R	x_β (nm)	K^0_{off} (s^{-1})	T^0_{off} (s)
Relationship: Maximal detachment force-ln(global loading rate)	Whole data set:						
	$n = 187$	280	-1.22×10^3	0.6	0.015	0.28	3.52
	($n = 332$)	*(342)*[a]	*(-1.36×10^3)*	*(0.57)*	*(0.012)*	*(0.16)*	*(6.4)*
	Three-point method						
	$n = 3$	379	-2.13×10^3	0.99	0.011	0.73	1.37
	($n = 3$)	*(467.4)*	*(-2.48×10^3)*	*(0.94)*	*(0.009)*	*(0.43)*	*(2.34)*
		Slope ($\sim f_\beta$) (pN)	Intercept (pN)	R	x_β (nm)	k^0_{off} (s^{-1})	t^0_{off} (s)
Relationship: Individual rupture force–ln(local loading rate)	Whole data set:						
	$n = 50$	45	–170.8	0.77	0.092	1.02	0.98
	($n = 171$)	*(29.7)*	*(–88.1)*	*(0.69)*	*(0.138)*	*(0.65)*	*(1.53)*
	Three-point method						
	$n = 3$	61	–293.7	0.99	0.067	1.94	0.52
	($n = 3$)	*(40.3)*	*(–160)*	*(0.98)*	*(0.102)*	*(1.32)*	*(0.76)*

[a]*Control values in parenthesis.*

moderately modified (lowered by CyaA toxin because k^0_{off} is increased) while its position moves inwards (x_β is decreased).

Discussion

The CyaA toxin is known to invade a wide range of eukaryotic target cells in which it produces high levels of cAMP thus altering the cellular physiology (Ladant and Ullmann, 1999; Vojtova et al., 2006; Carbonetti, 2010; Eby et al., 2010). Our results show that cAMP increases by order(s) of magnitude when AEC line (A549) are exposed to CyaA toxin (Figure 1C). CyaA toxin has been extensively studied for its molecular specificity and a unique mechanism of action (Ladant and Ullmann, 1999; Vojtova et al., 2006; Carbonetti, 2010). Most particularly, due to a very specific mode of intoxication (direct translocation of the catalytic domain through the plasma membrane of the host cell), CyaA intoxication is rapid, producing increase in cAMP within seconds, letting CyaA toxin play a key role in the early phase of respiratory tract colonisation (Ladant and Ullmann, 1999; Vojtova et al., 2006; Carbonetti, 2010).

The first important information presently obtained by the MFS method used here is that AECs shortly exposed to patho-physiological (small) dose of CyaA – not compromising cell viability – show that integrin-mediated cellular adhesion and to a lesser extent cell mechanics, are affected. This cytotoxic effect of CyaA occurs although A549 cells do not express the $\alpha_M\beta 2$-integrin receptors which are classically targeted by CyaA for initial interactions with host (immune) cells. Interestingly, these alterations in cell adhesion and cell mechanics properties are measurable in conditions where no significant alteration of cell viability is detected. In contrast, at high doses (supra-physiological) of CyaA toxin, the degradation of cell structure, cell viability and cell function is clearly evident. Importantly an enzymatically inactive form

Figure 6 | MFS results for local parameters obtained at various indentation/retraction speeds
In (**A**) the local rupture forces f^*(in pN) and in (**B**) the histograms of f^* (in pN) for the three different predetermined retraction speeds ($v = 2$, 5 and 10 μm/s) in control condition or for exposure to CyaA toxin concentrated at 0.5 nM. For each speed, the differences between cells exposed to CyaA toxin relatively to control conditions are significant ($p < 0.001$). A Gaussian distribution is observed for CyaA toxin at $v = 2$ and 5 μm/s. For (**A**), the squares in rectangular boxes mark the mean value, whisker bars the ±SD values, and the horizontal line in each box gives the median value. *$p \leq 0.05$; **$p \leq 0.01$; ***$p \leq 0.001$.

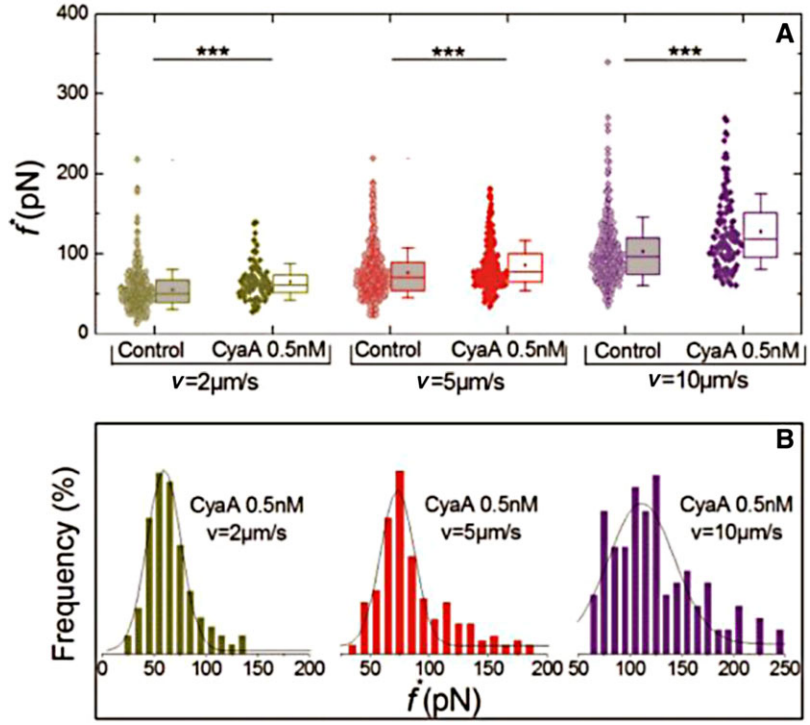

of CyaA (CyaAE5) has no effect on the measured adhesion and mechanical parameters indicating that the cAMP increase induced by CyaA is the cause of the measured cellular changes (Figure 3).

The second interesting information brought by the present results concerns the type of modifications induced by CyaA in terms of failure of increase in the number of bonds associated, thus restraining the early phase of adhesion reinforcement. It appears that CyaA toxin – even at the smallest (patho-physiological) concentration of 0.5 nM – compromises this reinforcement by systematically decreasing the strength of newly formed collective adhesion system created at the early phase of integrin–ligand interactions. At the same time, we observe that cell height is increased, F-actin structure is affected and apical cell stiffness is increased. The advantage of the MFS approach compared with the more classical single bond force spectroscopy (FS) methods (Lehenkari and Horton, 1999; Taubenberger et al., 2007) is to assess the CyaA-induced modifications in terms of bond structure and the number of non-cooperative associated bond breaking stochastically (see Material and Methods). Indeed, the theoretical predictions described in this paper show that the number of bonds (here, the integrin receptors) implicated in the cell-probe adhesion can be estimated from the ratio $N = F_\beta / f_\beta$ for cells invaded by CyaA toxin and for control conditions. From this simple expression, we find: $N \approx 6$ after CyaA exposure and $N \approx 12$ (Table 1) in control conditions. It means that CyaA intoxication tends to markedly decrease the number of newly formed bonds generated at the apical cell surface by cell

Figure 7 | Force–loading rate relationship at the local level
The relationship between the rupture forcef^* (in pN) and the local loading rate r_f (in pN/s) plotted on natural logarithmic scale and calculated for CyaA toxin at 0.5 nM concentration and for the three predetermined speeds: $v = 2$ μm/s (green points), $v = 5$ μm/s (red points) and $v = 10$ μm/s (purple points). The slope of the linear regression (continuous line) gives the reference force f_β and the intercept with vertical axis at r_f 1 pN/s enables to calculate the natural dissociation rate k^0_{off} (in s^{-1}) from the relation: $[f^*]_{\ln r_f=0} = -f_\beta \ln(k^0_{off} f_\beta)$. The dotted line represents the linear regression for control condition. Note that points of control condition are not plotted on this graph.

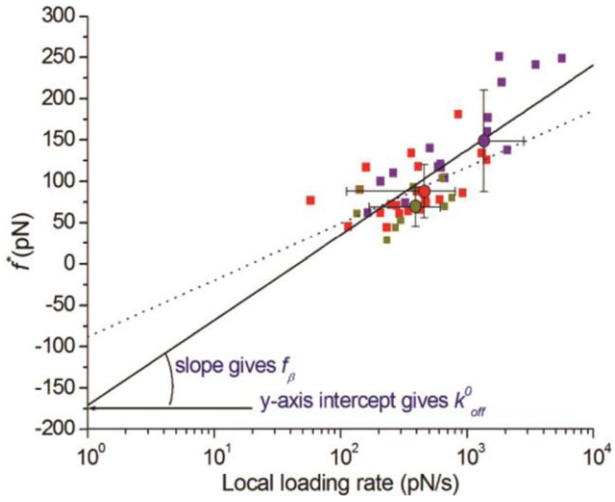

interaction with the coated probe. This decay in estimated adhesion bonds suggests that integrin clustering might be reduced in presence of CyaA toxin while analysis of individual rupture events show that adhesion energy of individual integrin–ligand bonds is only moderately affected (see *Results* and values of f_β and k^0_{off}in Table 1). In a consistent fashion, the range of local rupture forces found in cells exposed to CyaA (≈70–150 pN; see Supplementary Table 2) is only slightly above that found in control conditions (≈60–115 pN; see Supplementary Table 2) likely because loading rates during CyaA exposure tend to be higher (cells are becoming stiffer) (see Supplementary Table 2). Incidentally, the range of local force rupture found in A549 is in agreement with the range of rupture forces (40–100 pN) found with a method allowing to characterise single-integrin unbinding rupture events at the early phase of adhesion (Taubenberger et al., 2007). In summary, the CyaA-induced adhesion weakening found at global cell scale would be essentially due to the decay in bond number association caused by CyaA intoxication and not really by a CyaA-induced change in chemical energy of the integrin–ligand binding.

Concerning the experimental conditions presently used with the MFS method, it should be indicated that to determine the bond number of the newly formed integrin adhesion systems, we needed to limit the range of loading rate to 2 decades. Using a 3-decade range of loading rates, Zhang et al. (2004) found two activation potential energy barriers (a steep inner barrier and a more elevated outer barrier) for the integrin $\alpha_4\beta_1$–vascular cell adhesion molecule-1 (VCAM-1) system. Indeed, in the case where the adhesion system must overcome a series of increasingly higher energy barriers before final dissociation, the dissociation kinetics of the complex at low loading rates is governed by the properties of the outmost barrier (Li et al., 2003). Nevertheless, the outer barrier is the site of integrin activation and the most relevant energetic site for newly formed bonds implicated in adhesion reinforcement. By contrast to previous approaches on integrin receptors which could not provide the bond number per adhesive unit (Taubenberger et al., 2007), the present MFS method offers this new possibility. Noteworthy, in our cellular model of CyaA intoxication, it is precisely the number of newly formed bonds which is affected by cytotoxicity of CyaA.

A third important aspect highlighted by the present study is the ability of the CyaA toxin to efficiently invade A549 cells that are human alveolar basal epithelial cells. Although these cells do not express the $\alpha_M\beta_2$ integrin (Massin et al., 2004; Merilahti et al., 2016), the primary CyaA receptor on innate immune cells (Guermonprez et al., 2001), we show here that CyaA, at concentrations (0.5 nM) that are expected to be reached *in vivo* at the surface of an epithelium colonised by *B. pertussis* (Eby et al., 2013), elicits a substantial increase in intracellular cAMP and significantly alters the cell bio-mechanics and adhesion properties. These data thus suggest that in addition to the well-established and general role of CyaA in counteracting the innate immune responses thus facilitating the host colonisation by *B. pertussis*, CyaA may also have a local effect on the epithelium colonised by the bacteria. Eby et al.

Figure 8 | Sketch of the MFS method

Procedure for measuring adhesion and mechanical parameters by multiple bond force spectroscopy (MFS) method using AFM. (**A**) Typical time-dependent signal of force (in nN) recorded on AFM device showing the sequence of successive manoeuvres (in relation to the probe position relatively to the cell sketched on top) used during an MFS experiment. Three characteristic periods can be observed: (i) Approach and indentation of a RGD-coated spherical probe at predetermined constant speed ($v = 5\ \mu$m/s on this record) up to a maximal pressing force of 5 nN (red part of the curve), (ii) cell contact during 2 s and a contact force set at 5 nN (green part of the curve), (iii) retraction obtained at the same predetermined constant speed (5 μm/s on this record) (blue part of the curve). (**B**) Typical force–distance curve obtained in a given A549 cell showing the indentation period (red curve) and the retraction period (blue curve). The Young modulus is obtained by Hertz model in the low range of indentation ($<0.5\ \mu$m), whereas global and local adhesion parameters are obtained on the retraction curve. The adhesion parameters are: (i) the maximal detachment force F^*in nN range (or global rupture force) which corresponds to peak (negative) value recorded on the retraction curve and the work of adhesion W_{adh} in nN $\times\ \mu$m calculated from the striped area, (ii) the local rupture force f^* (step increase) which aims at characterising (see insert) the single-bond rupture forces (in pN range) and the local cellular/molecular stiffness (k_{local}) from the negative slopes preceding the local bond ruptures. In case of a zero slope (plateau) which is attributed to tether extension with no measurable cell stiffness, the local loading rate could not be estimated and the rupture force data did not enter in the statistics of the loading rate dependence of rupture force f^*.

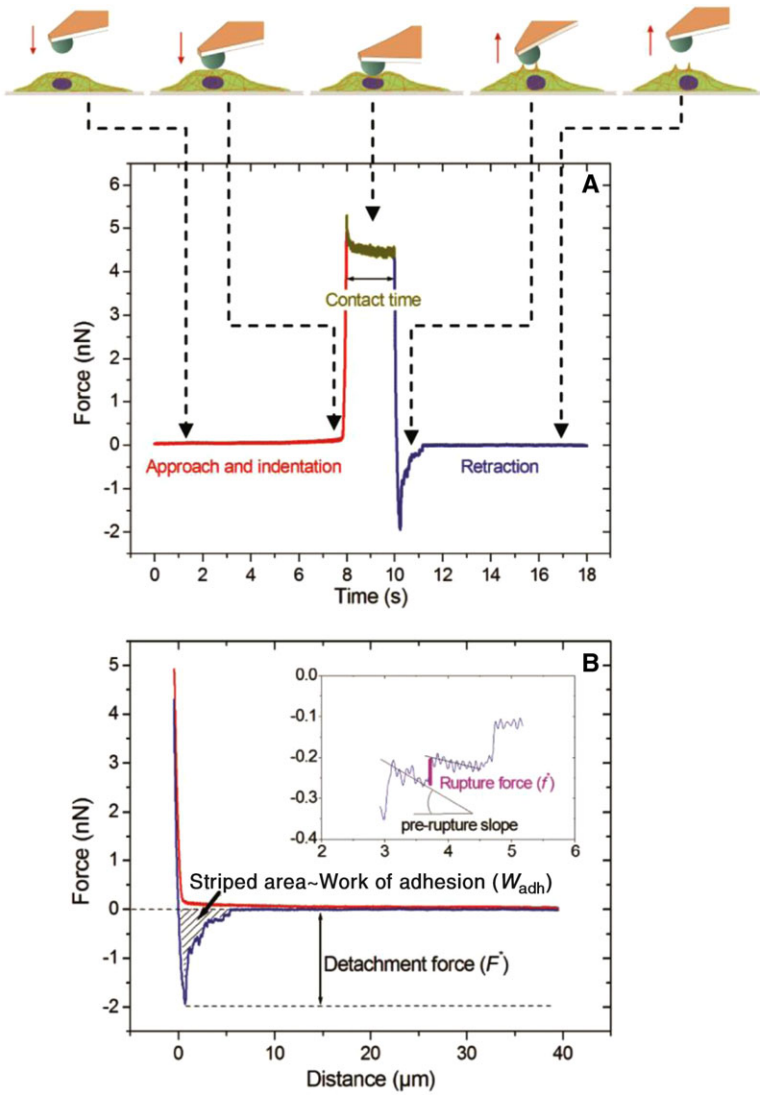

(2010) previously reported that CyaA could invade polarised T84 cell monolayers or human airway epithelial cultures when applied to their basolateral membranes (Eby et al., 2010). These polarised epithelial cells model the mucosal surface of the host, while the A549 cells are characterised by an alveolar epithelial phenotype and do not have a protective mucosal surface. Hence, various epithelial cell types could be targeted by CyaA during the course of bacterial infection. The direct, cAMP-mediated effects of CyaA on the mechanics (increase in Young's modulus) and adhesion properties of the intoxicated cells, as evidenced here, may thus contribute to the alteration of lung epithelia, a characteristic of the *B. pertussis* infection.

Material and methods

Preparation of A549 AECs

A549 are human AECs (ATCC) issued from a human lung carcinoma but having the phenotype of alveolar type II epithelial cells. When forming a monolayer, A549 cells adopt a phenotype consistent with type II AECs *in vivo* and, importantly do not functionally differentiate in culture from type I AECs. They have the ability to form adherent and tight junctions when grown to confluence, and they offer many advantages for studying *in vitro* the patho-physiological response of AECs. These cells express a wide variety of cytokines, growth factors and receptors and notably several transmembrane receptors of the integrin type: β_1, α_3, α_6, α_5 and α_2 (Massin et al., 2004). In addition, integrin subunits α_V associated with integrin subunits β_3 and β_6 are expressed in A549 cells (Merilahti et al., 2016). These integrin receptors bind the synthetic peptide containing the RGD sequence present in many extracellular matrix components. Indeed, the specificity of RGD-binding integrins include five integrin subunits α_V ($\alpha_V\beta_1$, $\alpha_V\beta_3$, $\alpha_V\beta_5$, $\alpha_V\beta_6$ and $\alpha_V\beta_8$), two β_1 integrin subunits ($\alpha_5\beta_1$ and $\alpha_8\beta_1$) and $\alpha_{IIb}\beta_3$ (Humphries et al., 2006), most of these subunits being expressed by A549 cells but at a level which depends on the passage number: the lower the passage number, the higher the level of integrin expression (Sean et al., 2010). Here, passage number stays in the low range (≈12–16). A cyclic RGD peptide is used instead of proteins because peptide generates no immune response, no infection risk, better stability, more simple orientation and single adhesion motif (Hersel et al., 2003).

Cells were cultured in T25 flasks (TPP) with 5 ml of complete medium containing DMEM-Glutamax High glucose medium (Gibco Life technologies), 1% penicillin/streptomycin (Sigma–Aldrich) and 10% foetal bovine serum (Sigma–Aldrich) under controlled atmosphere (37°C, 5% CO_2, 95% air). To subconfluence, cells were washed with PBS without calcium and magnesium ions or $PBS^{-/-}$ (Gibco Life technologies), then trypsined with 0.5 ml Trypsin-EDTA (Sigma–Aldrich) and incubated at controlled atmosphere for 2 min. After that, trypsin was inactivated by 5 ml of fresh complete medium.

For subculturing in T25 flasks, a split ratio of 1/10 was used. For experiments, we used a density of 7.10^5 cells and seeded on petri-dish (TPP Ø34 mm) coated with fibronectin at 10 ng/mm². The culture of A549 reached confluence in 24 h in complete medium. Once cells reach confluence state, that is practically when cells cover more than 90% of the surface – the culture medium is replaced by a culture medium without serum and with 0.5% of BSA first to stop cell proliferation, second to eliminate all not known compounds present in the serum than might interfere with the CyaA treatment, and third to increase the specificity of bead binding at the cell surface. Thirty minutes before experiments, cells were incubated in serum free medium supplemented with 0.5% BSA to block the non-specific binding (Planus et al., 1999).

Production and purification of CyaA and inactive variant CyaAE5

CyaA and the enzymatically inactive variant CyaAE5 (resulting from a LQ dipeptide insertion between D188 and I189 in the catalytic core of the enzyme (Ladant et al., 1992) were expressed in *E. coli* and purified to near homogeneity by previously established procedures (Guermonprez et al., 2001; Karst et al., 2014). Succinctly, the inclusion bodies were solubilised in 50 ml of 20 mM Hepes, 8 M urea, pH 7.4 by overnight solubilisation under constant stirring at 4°C. A centrifugation for 20 min at 1200 rpm enables to extract the supernatant which is supplemented with 0.14 M NaCl and then incubated for 1 h at RT with 75 ml of Q-Sepharose resin equilibrated with 20 mM Hepes, 140 mM NaCl, 8 M urea, pH 7.4. The Q-Sepharose resin, retaining the CyaA protein, is loaded onto a column. After an extensive wash to eliminate contaminants, the CyaA protein is eluted in 20 mM Hepes, 500 mM NaCl, 8 M urea, pH 7.4. After dilution of the eluate in 20 mM Hepes and 8 M urea, it is loaded onto a second Q-sepharose column. Washing and elution are operated in the same conditions as the first time. This step allows to obtain a concentrated CyaA protein which is diluted five times then with 20 mM Hepes, 1 M NaCl, pH 7.4 and loads onto a 70 ml phenyl-sepharose column and washes with 20 mM Hepes, 1 M NaCl, with Hepes 20 mM again and then with 50% isopropanol. After an extensive wash, the toxin is eluated with 20 mM Hepes and 8 M urea. In a final step, the eluate is applied onto a sephacryl 500 (GE healthcare, HIPREP 26/60) equilibrated in 20 mM Hepes and 8 M urea. CyaA batches are pooled and concentrated by ultrafiltration and stored at −20°C in 20 mM Hepes and 8 M urea. CyaA toxin concentrations are determined by spectrophotometry using a molecular extinction coefficient at 280 nm, Em_{280} = 143,590 M^{-1} cm^{-1}, which is computed from the CyaA sequence on the ProtParam server (http://web.expasy.org/protparam/). The purity of CyaA batches is higher than 90% as judged by SDS-PAGE analysis and contained less than 1 EU of LPS/μg of protein as determined by a standard LAL assay (Lonza). Finally, CyaA is refolded into a urea-free, monomeric and functional holo-state (Karst et al., 2014) on a BioSEC5 21.2 * 300 mm with a 5 ml G25-SF as pre-column. The refolding efficiency is around 40 ± 5% (population monomer/total population of proteins). The biological functions, that is haemolysis, translocation of ACD and cAMP production, are routinely assayed as described in Karst et al. (2014) and Cannella et al. (2017). The aliquots of monomeric

species of CyaA are stored at −20°C in 20 mM Hepes, 150 mM NaCl, 2 mM $CaCl_2$, pH 7.4.

Handling of CyaA and CyaAE5 toxins

For our experiments, CyaA and CyaAE5 toxins are diluted into a solution containing 97% of BSA-DMEM without red phenol medium, 2% of buffer and 1% of $CaCl_2$, of the total volume, which is essential for the activation of these toxins. CyaA/CyaAE5 mixture is added 15 min prior to the experiment. Due to the sequential character of AFM experiments, the CyaA/CyaAE5 exposure time varies from cell to cell in the range from 15 min to approximately 60 min. We used a range of concentration of CyaA/CaAE5 toxin from 0.5 to 10 nM.

cAMP assays

A549 cells are plated at 3.10^5 cells per well and exposed to control conditions or to three CyaA concentrations (0.5, 5 and 10 nM) or to three CyaAE5 concentrations (0.5, 5 and 10 nM) for 30 min. Intracellular cAMP concentration has been determined with the Cyclic AMP Competitive ELISA kit (Invitrogen) according to the manufacturer's instructions.

Viability test

The Trypan blue is a vital stain used to selectively colour dead cells which is used only for the viability test and not for AFM experiments. The colourant penetrates and stays only in dead cells which are not able to eject it. Indeed, this mechanism requires energy that live cells provide by mitochondria to eject it. Practically, the Trypan blue (Sigma–Aldrich) is added to cell suspension which was previously exposed or not to CyaA toxin (0.5, 5 and 10 nM). Then, specifically for the cell counting procedure, we discriminated live cells (no colour) and dead cells (in blue) by counting with Malassez Single cell to obtain viability percentage: (live cell number/total cell number) × 100.

Actin cytoskeleton and focal adhesion staining

A549 cells are plated at 100,000 cells/ml on coverslip (Ø 18 mm). After 24 h at 37°C and 5% CO_2, cells reach 60% of confluence and are exposed during 30 min to different conditions: control (complete medium and CyaA activation buffer) and CyaA toxin (toxin and CyaA activation buffer) at three different CyaA concentrations: 0.5, 5 and 10 nM. Then, cells are washed three times with PBS. Cells are right after fixed 10 min with 4%-paraformaldehyde. This short phase occurs with diluted solution of paraformaldehyde which greatly limits the impact on observed structures. Cells are washed three times with PBS and then permeabilised by 0.3% Triton during 10 min. This step allows antibodies to access to intracellular antigens and requires the use of a detergent such as Triton X-100. Cells washed three times with PBS are hereafter incubated for 30 min with PBS containing 1% of BSA in order to block non-specific sites. After removing blocking solution, cells are incubated 1 h at room temperature (RT) in diluted phospho-tyrosine PY99primary antibody solution (sc-7020; Santa Cruz Biotechnology; dilute at 1/150) to stain the focal adhesion points. Cells are then washed three times with a solution containing PBS and 0.02% Triton and incubated 1 h at RT in dark in diluted fluorochrome-conjugated secondary antibody (Alexa-488; Life Technology; dilute at 1/1000) to reveal in the green colour, the staining of focal adhesion points. After a new cell washing repeated three times with PBS-0.02% Triton cells are incubated in diluted Phalloidin Tetramethylrhodamine B-isothiocyanate solution (Sigma; dilute at 1/2000) to stain F-actin in the red colour. Cover slides were mounted on a slide with the cell side down in Prolong (Life Technology). Staining structures are observed and images are acquired on an Axio Imager confocal microscope (Zeiss) at 63× magnification. To analyse cellular images, the mean level of fluorescence of F-actin is determined in each cell by automatic quantification by ImageJ software relatively to the fluorescent background level of each image. After subtraction, we obtain the effective mean fluorescence of the cells. To determine the number of focal adhesion points, the phospho-tyrosin PY99 level is analysed using a thresholding method and the automatic particle analyser in ImageJ software. On these same cover slides, confocal microscope with the LSM5 Pascal software was used to perform z-stack images of fluorescent cellular planes every 0.5 μm and then 3D-reconstructions to estimate cell height for each tested condition.

AFM measurements by integrin-specific cellular probing

FS was conducted using commercial NanoWizard 1 AFM (JPK Instruments) on cells showing a characteristic shape of adherent epithelium without any blebs, or cellular damage (cells in ball shape or cells partially or totally detached from the culture, are not chosen; see Supplementary Figure 1). The AFM is settled on the AxioObserver Z1 inversed microscope (Zeiss) equipped with a Zeiss EC-Plan-NEOFLUAR 20× lens. The microscope is placed on a stabilisation table TL-150 (Table Stable Ltd.) so that most vibration sources are minimised. The CellHesion module (JPK Instruments) comprising an electronic controller and a piezo-driven stage enables a vertical displacement up to 100 μm. The DirectOverlay^{TM} system (JPK Instruments) uses the accuracy of the AFM closed-loop scanning system to enable a perfect match of the optical and AFM images in such way that the cellular position of the FS manoeuvres can be selected from the optical image (Supplementary Figure 1). FS measurements are performed on the cell membrane above the relatively flat nuclear region, that is where the cell thickness is always the highest (>3.5 μm; see Supplementary Figure 2) thus minimising the influence of the substrate (Domke and Radmacher, 1998) and the influence of intracellular variability, while the contact geometry rather well defined. A unique force curve per cell is intentionally performed in order to minimise cell adaptation response that might be induced by a repeated mechanical stimulation (Tamada et al., 2004). For each condition tested, about 40–60 different cells are selected.

FS measurements are carried out with a 6.6 μm spherical probe SquBe CP-CONT-SiO-C (Nanoandmore) mounted on a cantilever whose stiffness is in the range of 0.02–0.77 N/m (average cantilever stiffness value: 0.5 N/m). To take into account this variability, all cantilevers are systematically calibrated prior to FS experiment by the thermal noise oscillator method (Butt and Jaschke, 1995). The spherical shape of the probe is chosen to avoid any membrane injury.

AFM cantilever, after a preliminary cleaning with Triton 0.5% and ethanol, is systematically treated with air-based plasma (Harrick Plasma Cleaner-PDC-002-HPCE). This step makes the probe surface hydrophilic and thus energetically available

for contact with the aqueous coating solution. The probe is then sterilised under UV exposure for 25 min, functionalised with 2.5 mg/ml RGD solution and finally stored at 4°C for 1 night. Before being mounted on the cantilever holder, the probe is thoroughly rinsed with PBS in order to eliminate unbound RGD peptides.

A typical FS cycle comprises three phases depicted in Figure 8A: (i) Approach: the piezo moves the stage upwards so that the cell is brought into contact and the probe deforms the cytoplasm until a point of maximum effort is reached, that is contact force = 5 nN; (ii) Contact: the stage is immobilised during a predetermined contact time which is set at 2 s to enable studying adhesion in its early phase; these contact conditions were chosen after preliminary experiments which permitted to define the best compromise between a sufficient number of rupture events and complete bond rupture during the retraction period; (iii) retraction (detailed in Figure 8B): at the end of the contact time, the piezo moves the stage downwards at the same constant speed as approach, the probe is progressively separated from the cell, the bond(s) created at the extremity of cellular extensions break randomly thereby generating sudden steps throughout the retraction force–curve. It should be indicated here that the binding system generated during such short contact time (2 s + a few seconds of retraction manoeuvre duration; see Figure 8A) corresponds to the early phase of integrin binding and thus is markedly different from the mature cell–substrate focal adhesion system observed by immunostaining (see previous paragraph).

The cantilever speed is kept constant at three predetermined values: v = 2, 5 and 10 μm/s. This speed range is purposely limited (i) towards low values to minimise the duration of FS experiments (maximum half a minute per cell) and thus to avoid cell morphological changes, and (ii) towards high values to guaranty quasi-static conditions and minimal hydrodynamic friction on the probe. Indeed, due to the moderate range of approach and separation speeds used in this study, the hydrodrag is negligible (a few % maximum) for the two lowest speeds tested (2 and 5 μm/s) and, is smaller than 10 pN for the highest speed tested (10 μm/s). This leads to an error on the measured rupture forces lower than 10%, letting the hydrodrag correction unnecessary in present experimental conditions. Closed-loop system is activated in order to precisely control the z-movement. The z-movement of 35 μm from contact point leads to the total separation of the probe from cells in most of presently studied cases. The sampling rate is set at 1 kHz allowing capturing rapid change in signal.

Multiple and single bond analysis

We consider that the cellular adhesion system created between the adherent cell and the coated probe – presently a 6.6 μm-diameter spherical probe coated for specific integrin binding – is a complex bond system, that is containing a number of N constitutive integrin–ligand junctions with individual energy barriers. The Kramer–Smoluchowski theory (Evans, 1998, 2001; Tsukasaki et al., 2007) predicts that the global lifetime needed to transit across such a complex energy barrier can be expressed as the sum of the individual times needed to transit across each energy barriers. The inverse of the global lifetime is the global dissociation rate, noted $K_{\text{off}}(f)$ which can thereby be expressed in terms of individual dissociation rates. Assuming that individual barrier height are all identical meaning similar integrin–ligand bonding due to the integrin-specific probe coating treatment, the individual dissociation rates are thus equivalent and noted $k_{\text{off}}(f)$. Accordingly:

$$K_{\text{off}}\left(f\right) = \frac{1}{\sum_{n=1}^{N}\left[k_{\text{off}}\left(f\right)\right]^{-1}} \tag{1}$$

Considering two typical configurations of bonds working non cooperatively (*i.e.* breaking randomly), namely zipper and parallel as previously done (Evans, 2001; Williams, 2003), we recently demonstrated (Isabey et al., 2013) that the global lifetime can be written in the form of a generalised Bell's model (Bell, 1978) with a prefactor called global natural dissociation rate K_{off}^{0} and an exponent representing the separating force f normalised by a global force scale noted F_β:

$$K_{\text{off}}\left(f\right) = K_{\text{off}}^{0}\exp\left(\frac{f}{F_\beta}\right) \tag{2}$$

For each individual bond, the bond kinetic parameters are classically given by a similar expression:

$$k_{\text{off}}\left(f\right) = k_{\text{off}}^{0}\,\exp\left(\frac{f}{f_\beta}\right) \text{ with } k_{\text{off}}^{0} = \frac{1}{t_{\text{D}}}\exp\left(-\frac{E_{\text{b}}}{k_{\text{B}}T}\right) \text{ and } f_\beta = \frac{k_{\text{B}}T}{x_\beta} \tag{3}$$

k_{off}^{0} represents the natural dissociation rate of an individual bond which is related to the height of the chemical energy barrier E_{b} in the absence of force, $k_{\text{B}}T$ is a thermal energy scale (= 4 pN×μm), t_{D} is the Brownian time (= 10^{-9}–10^{-10} s), x_β is the distance (in the nm range) at which the energy barrier is located (called transition state).

The relationship between the global adhesion parameters: K_{off}^{0}, F_β and the individual adhesion parameters: k_{off}^{0}, f_β, depends on the bond configuration. Parallel configuration appears to be the appropriate bond model for FS experiments (Isabey et al., 2013; Nguyen et al., 2017). Indeed, during AFM experiments, the force applied on the bonds created between the bead and the cell is exerted perpendicularly to the plane of cell culture, and the force, f applied on the collective bond, has more chance to be homogeneously distributed between existing bonds and force distribution likely remains uniform up to the total rupture of the bond system (Sulchek et al., 2005; Rankl et al., 2008). For parallel bonds, K_{off}^{0} depends on the force level f uniformly distributed on all bonds:

$$K_{\text{off}}^{0} \approx \left(\frac{k_{\text{off}}^{0}}{\ln N}\right)_{F\to 0} \text{ or } K_{\text{off}}^{0} \approx \left(k_{\text{off}}^{0}\sqrt{2}\left(\frac{f}{N f_\beta}\right)^{0.5}\right)_{N\geq 2;F\neq 0} \tag{4}$$

Eq. (4) means that K_{off}^{0} decreases slightly with N and $F_\beta = N f_\beta$, i.e. F_β is proportional to N which means that an increase in bond number induces an exponential increase in the global bond lifetime, and therefore an exponential decrease in the global dissociation rate, $K_{\text{off}}(f)$ (Equation (2)).

In addition, during AFM experiments, bonds can normally be stretched under a constant loading rate $r_{\text{f}} = \text{cste} = df/dt$, the profile of dissociation kinetics under force may be obtained (Evans and Kinoshita, 2007), leading to the calculation of the most probable rupture force for individual bonds. For complex bonds, we used the analytical expressions of $K_{\text{off}}(f)$ proposed

for the parallel configuration in (Isabey et al., 2013), leading for to the following expression of the global rupture force F^*(also called in the literature: "maximal detachment force"):

$$F^* = F_\beta \ln\left[\frac{r_f}{K_{off}^0 F_\beta \left(\frac{2}{2+F_\beta/F^*}\right)}\right] \approx F_\beta \ln\left[\frac{r_f}{K_{off}^0 F_\beta}\right] \quad N \geq 2 \quad (5)$$

Eq. (5) shows that the rupture force of a complex parallel bond, F^*, is approximately proportional to the logarithm of the loading rate as for single bonds (Evans and Ritchie, 1997; Evans, 1998). It should be indicated here that the role of the surrounding mechanical environment on strength of a collective bond is actually taken into account through the loading rate dependency described by Eq. (5). Noteworthy, F^*increases almost proportionally with N through $F_\beta = N f_\beta$ if an appropriate estimate of the loading rate can be performed. If this can be done, the $F^* - \ln[r_f]$ relationships enables to calculate global reference force,F_β, and beyond an estimate of the bond number N if an appropriate estimate of the individual reference force f_β can also be performed. Since a similar expression, that is $f^* \approx f_\beta \ln[\frac{r_f}{k_{off}^0 f_\beta}]$ (Evans and Ritchie, 1997; Evans, 1998) can be applied to the analysis of individual rupture events (except that the loading rate r_f is the actual loading rate preceding the single bond rupture), the slope of the linear relationship $f^* - \ln[r_f]$ enables to estimate the reference force, f_β. Moreover, the value of the natural dissociation rate K_{off}^0 can be obtained from the intercept between this regression line and, for example the vertical axis ($[F^*]_{\ln r_f=0} = -f_\beta \ln(K_{off}^0 F_\beta)$). A similar approach used for the single bond leads to an estimate of k_{off}^0.

The adhesion reinforcement permitted by the collective (parallel) bond configuration can thereby be evaluated through a characterisation of bond number by comparing the $\ln(r_f)$-dependence of rupture forces (i) in a multiple bond system (F^*) and (ii) in the individual bonds f^* which properly constitute the tested multiple bond structure. This comparison can be performed by AFM throughout a given FS curve to the extent that this curve contains – not one as in standard single bond FS (Taubenberger et al., 2007) – but several bond rupture events as found in present experiments (see records of FS curves obtained for three different CyaA concentrations in Supplementary Figure 3) . This requires that a multiple bond system has been created between the AFM probe and the cell (Figure 8B). Such a method called MFS is described in a companion paper (Nguyen et al., 2017) and is used in the present study to evaluate the effect of CyaA toxin on cell mechanics and cell adhesion in its early phase.

Determination of loading rate and adhesion parameters from force–distance curves

Based on Evans and Ritchie (Evans and Ritchie, 1997, 1999) the loading rate can be estimated from the product of the retraction speed v (constant in a given AFM experiments) by the effective stiffness:

$$r_f = \frac{df}{dt} = \frac{df}{dx}\frac{dx}{dt} = k_{eff} v \quad (6)$$

The parameter $k_{eff} = [\frac{1}{k_{cant}} + \frac{1}{k_{cell}}]^{-1}$account for the AFM cantilever stiffness k_{cant} on one side of the bond, and on the stiffness k_{cell} of the cellular structure connected on the other side (cell cortex, tensed actin filaments ... etc) (Odorico et al., 2007). In present experiments, $k_{cant} >> k_{cell}$ leading to $k_{eff} \approx k_{cell}$ hence:

$$r_f = k_{cell} v \quad (7)$$

In present experiments, the cellular stiffness k_{cell} was determined at global and local scales:

i. At the global cellular scale, from the product of a characteristic cell deformation scale (calculated cell-by-cell as indicated in Supplementary Table 2) and of the Young's modulus E_{cell} whose value is estimated at small deformation, that is in the initial portion of the curve (cell indentation/cell height $\approx 0.5\ \mu$m/5 μm $\approx 10\%$ deformation) using the Hertz model (Kuznetsova et al., 2007) and assuming an infinitely rigid probe material. If F is the known vertical indentation force, h the indentation depth, E_{cell} is obtained from: $F \approx \frac{16\sqrt{R}}{9} E_{cell} h^{3/2}$. Note that in the low deformation range, indentation and retract curves are supposed to lead to similar values of Young's modulus (Bulychev et al., 1975).
ii. At the local cellular/molecular level by the slope of a straight line fitted through the final part of the retract force-displacement curve preceding the point of bond rupture (see insert in Figure 7B) as earlier proposed by several authors (Li et al., 2003; Taubenberger et al., 2007). This slope provides an estimate of the local cellular/molecular stiffness right before local bond rupture. The local loading rate is obtained by Eq. (6), assuming that the retraction speed v is preserved throughout any of the local cellular extensions.

Global and local adhesion properties are determined directly from the retraction curve. The global properties are the detachment force F^* defined by the maximal absolute value of force, and the work of adhesion W_{adh} defined as the area delimited by the retraction curve and the x-axis (Figure 8B). The work of adhesion W_{adh} is a convolution of cell mechanics and cell adhesion energies needed to reach complete separation of the probe from the cell. In that sense, W_{adh} integrates all mechanical and rupture events contributing to the link between the probe and the cell. The local bond rupture events are quantified from the height of the force steps visible on the retraction curve and by the negative slope preceding the rupture event (Figure 1B, insert). Each force step represents the individual bond rupture events, each bond contributing to the global adhesion properties characterised by F^* . The slope gives the local rigidity of the subcellular system to which the individual bonds are attached.

Statistical tests and plots

Comparison of the mean values of mechanical and adhesion parameters between the different biological conditions tested was performed with statistical software package (Statistica v7.1, StatSoft, France) using Kruskal–Wallis non parametric test. A 1-, 2-, 3-star significance corresponds to P values smaller than 0.05, 0.01 and 0.001, respectively, depicted by black horizontal lines. Statistical plot type used in this article is box-whisker: dot in box marks the mean value, whisker bars the ±SD values, and horizontal bar in box gives the median value. Black horizontal lines show statistical significance. In bar graph, error bar are ±SEM values.

Author contribution

A.C. acquired and analysed data and wrote the paper. N.N.-M. conceived and performed the experiments, analysed data and wrote the paper. A.D.S. provided assistance in cell experiments and corrected the paper. P.E. provided expertise on cell biology and corrected the paper. P.G., L.B. and F.M. provided physical expertise, mathematical computation and paper proofreading. C.A. and L.D. provided the expertise, purified the toxin and proofread the paper, and I.D. designed and coordinated the study and wrote the paper.

Funding

For this research, we acknowledge receipt of grants from Institut Pasteur, CNRS UMR 3528, Agence Nationale de la Recherche (ANR n° 2010-BLAN-1119-05) and from Fondation pour la Recherche Médicale: FRM programme Bio-Ingénierie pour la Santé 2014 (DBS 20140930771).

Acknowledgements

The authors thank Emilie Bequignon, André Coste, Estelle Escudier, Jean-François Papon, for their helpful advice and the fruitful discussions.

Conflict of interest statement

The authors have declared no conflict of interest.

References

Ahmad, J.N., Cerny, O., Linhartova, I., Masin, J., Osicka, R. and Sebo, P. (2016) cAMP signalling of Bordetella adenylate cyclase toxin through the SHP-1 phosphatase activates the BimEL-Bax pro-apoptotic cascade in phagocytes. Cell Microbiol **18**, 384–398

Bell, G.I. (1978) Models for the specific adhesion of cells to cells. Science (New York, N.Y.), **200**(**4342**), 618–627

Bulychev, S.I., Alekhin, V.P., Shorshorov, M.K., Ternovskii, A.P. and Shnyrev, G.D. (1975) Determining Young's modulus from the indentor penetration diagram. Zavodskaya Lab. **9**, 1137–1140.

Butt, H. and Jaschke, M. (1995) Calculation of thermal noise in atomic force microscopy. Nanotechnology **6**, 1–7

Cannella, S.E., Yvette, V., Enguéné, N., Davi, M., Malosse, C., Cristina, A., Pérez, S., Chamot-rooke, J., Vachette, P., Durand, D., Ladant, D. and Chenal, A. (2017) *Stability, structural and functional properties of a monomeric, calcium – loaded adenylate cyclase toxin, CyaA, from Bordetella pertussis*. Scientific report. 1–17.

Carbonetti, N.H. (2010) Pertussis toxin and adenylate cyclase toxin: key virulence factors of Bordetella pertussis and cell biology tools. Future Microbiol. **5**(**3**), 455–469

Domke, J. and Radmacher, M. (1998) Measuring the elastic properties of thin polymer films with the atomic force microscope. Langmuir **14**(**18**), 3320–3325

Eby, J.C., Ciesla, W.P., Hamman, W., Donato, G.M., Pickles, R.J., Hewlett, E.L. and Lencer, W.I. (2010) Selective translocation of the Bordetella pertussis adenylate cyclase toxin across the basolateral membranes of polarized epithelial cells. J. Biol. Chem. **285**(**14**), 10662–10670

Eby, J.C., Gray, M.C., Warfel, J.M., Paddock, C.D., Jones, T.F., Day, S.R., Bowden, J., Poulter, M.D., Donato, G.M., Merkel, T.J. and Hewlett, E.L. (2013) Quantification of the adenylate cyclase toxin of bordetella pertussis in vitro and during respiratory infection. Infect. Immun. **81**(**5**), 1390–1398

Evans, E. (1998) Energy landscapes of biomolecular adhesion and receptor anchoring at interfaces explored with dynamic force spectroscopy. Farad. Discuss. (**111**), 1–16.

Evans, E. (2001) Probing the relation between force—lifetime—and chemistry in single molecular bonds. Annu. Rev. Biophys. Biomol. Struct. **30**(**1**), 105–128

Evans, E. and Kinoshita, K. (2007) Using force to probe single-molecule receptor-cytoskeletal anchoring beneath the surface of a living cell. Methods Cell Biol. **83**(**7**), 373–396

Evans, E. and Ritchie, K. (1997) Dynamic strength of molecular adhesion bonds. Biophys. J. **72**(**4**), 1541–1555

Evans, E. and Ritchie, K. (1999) Strength of a weak bond connecting flexible polymer chains. Biophys. J **76**(**5**), 2439–2447

Gray, M.C., Donato, G.M., Jones, F.R., Kim, T. and Hewlett, E.L. (2004) Newly secreted adenylate cyclase toxin is responsible for intoxication of target cells by Bordetella pertussis. Mol. Microbiol. **53**(**6**), 1709–1719

Gueirard, P., Druilhe, A., Pretolani, M. and Guiso, N. (1998) Role of adenylate cyclase-hemolysin in alveolar macrophage apoptosis during bordetella pertussis infection in vivo. Infect. Immun. **66**(**4**), 1718–1725.

Guermonprez, P., Khelef, N., Blouin, E., Rieu, P., Ricciardi-Castagnoli, P., Guiso, N., Ladant, D. and Leclerc, C. (2001) The adenylate cyclase toxin of bordetella pertussis binds to target cells via the alphaMbeta2 integrin (Cd11b/Cd18). J. Exp. Med. **193**(**9**), 1035–1044

Hersel, U., Dahmen, C. and Kessler, H. (2003) RGD modified polymers: biomaterials for stimulated cell adhesion and beyond. Biomaterials **24**(**24**), 4385–4415

Humphries, J.D., Byron, A. and Humphries, M.J. (2006) Integrin ligands at a glance. J. Cell Sci. **119**(**19**), 3901–3903

Isabey, D., Féréol, S., Caluch, A., Fodil, R., Louis, B. and Pelle, G. (2013) Force distribution on multiple bonds controls the kinetics of adhesion in stretched cells. J. Biomech. **46**(**2**), 307–313

Kamanova, J., Kofronova, O., Masin, J., Genth, H., Vojtova, J., Linhartova, I., Benada, O., Just, I. and Sebo, P. (2008) Adenylate cyclase toxin subverts phagocyte function by RhoA inhibition and unproductive ruffling. J. Immunol. **181**, 5587–5597

Karst, J.C., Enguéné, V.Y.N., Cannella, S.E., Subrini, O., Hessel, A., Debard, S., Ladant, D. and Chenal, A. (2014) Calcium, acylation, and molecular confinement favor folding of Bordetella pertussis adenylate cyclase cyaa toxin. J. Biol. Chem. **289**(**44**), 30702–30716

Khelef, N., Sakamoto, H. and Guiso, N. (1992) Both adenylate cyclase and hemolytic activities are required by Bordetella pertussis to initiate infection. Microb. Pathog. **12**(**3**), 227–235

Kuznetsova, T.G., Starodubtseva, M. N., Yegorenkov, N. I., Chizhik, S.A. and Zhdanov, R. I. (2007) Atomic force microscopy probing of cell elasticity. Micron (Oxford, England: 1993), **38**(**8**), pp. 824–33

Ladant, D., Glaser, P. and Ullmann, A. (1992) Insertional mutagenesis of Bordetella pertussis adenylate cyclase. J. Biol. Chem. **267**(**4**), 2244–2250

Ladant, D. and Ullmann, A. (1999) Bordetella pertussis adenylate cyclase: a toxin with multiple talents. Trends Microbiol. **7**(**99**), 172–176.

Lehenkari, P.P. and Horton, M.A. (1999) Single integrin molecule adhesion forces in intact cells measured by atomic force microscopy. Biochem. Biophys. Res. Commun. **259**(**3**), 645–650

Li, F., Redick, S.D., Erickson, H.P. and Moy, V.T. (2003) Force measurements of the alpha5beta1 integrin-fibronectin interaction. Biophys. J. **84**(**2 Pt 1**), 1252–1562

Massin, F., Rubinstein, E., Faure, G.C., Martinet, Y., Boucheix, C. and Béné, M.C. (2004) Tetraspan and beta-1 integrins expression pattern of the epithelial lung adenocarcinoma cell line A549 and its sensitivity to divalent cations. Cytometry B Clin. Cytom. **60**(**1**), 31–36

Merilahti, P., Tauriainen, S. and Susi, P. (2016) Human parechovirus 1 infection occurs via alphaVbeta1 integrin. PLoS One **11**(**4**)

Mouallem, M., Farfel, Z. and Hanski, E. (1990) Bordetella pertussis adenylate cyclase toxin: intoxication of host cells by bacterial invasion. Infec. Immun. **58**(**11**), 3759–3764

Nguyen, N.M., Angely, C., André Dias, S., Planus, E., Filoche, M., Pelle, G., Louis, B. and Isabey, D. (2017) Characterization of cellular adhesion reinforcement by multiple bond force spectroscopy in alveolar epithelial cells. Biol. Cell (accepted). 10.1111/boc.201600080

Odorico, M., Teulon, J.-M., Bessou, T., Vidaud, C., Bellanger, L., Chen, S.W., Quéméneur, E., Parot, P. and Pellequer, J.-L. (2007) Energy landscape of chelated uranyl: antibody interactions by dynamic force spectroscopy. Biophys. J. **93**(**2**), 645–654

Ohnishi, H., Miyake, M., Kamitani, S. and Horiguchi, Y. (2008) The morphological changes in cultured cells caused by Bordetella pertussis adenylate cyclase toxin. FEMS Microbiol. Lett. **279**, 174–179

Otero, A.S., Yi, X.B., Gray, M.C., Szabo, G. and Hewlett, E.L. (1995) Membrane depolarization prevents cell invasion by Bordetella pertussis adenylate cyclase toxin. J. Biol. Chem. **270**(**17**), 9695–9697

Planus, E., Galiacy, S., Matthay, M., Laurent, V., Gavrilovic, J., Murphy, G., Clérici, C., Isabey, D., Lafuma, C. and d'Ortho, M.-P. (1999) Role of collagenase in mediating in vitro alveolar epithelial wound repair. J. Cell Sci. **112**(**Pt 2**), 243–252

Qualmann, B., Kessels, M.M. and Kelly, R.B. (2000) Molecular links between endocytosis and the actin cytoskeleton. J. Cell. Biol. **150**(**5**), 111–116

Rankl, C., Kienberger, F., Wildling, L., Wruss, Jr., Gruber, H.J., Blaas, D. and Hinterdorfer, P. (2008) Multiple receptors involved in human rhinovirus attachment to live cells. Proc. Nat. Acad. Sci. U.S.A. **105**(**46**), 17778–17783

Sean, G., Barnes, R., Hawdon, N., Shewchuk, L., Eibl, J., Lam, J. and Ulanova, M. (2010) Up-regulation of integrin expression in lung adenocarninoma cells caused by bacterial infection: in vitro study. Innate Immun. **16**(**1**), 14–26

Sulchek, T.A, Friddle, R.W., Langry, K., Lau, E.Y., Albrecht, H., Ratto, T.V, DeNardo, S.J., Colvin, M.E. and Noy, A. (2005) Dynamic force spectroscopy of parallel individual Mucin1-antibody bonds. Proc. Nat. Acad. Sci. U.S.A. **102**(**46**), 16638–16643

Tamada, M., Sheetz, M.P. and Sawada, Y. (2004) Activation of a signaling cascade by cytoskeleton stretch. Dev. Cell **7**(**5**), 709–718

Taubenberger, A., Cisneros, D.A., Friedrichs, J., Puech, P.-H., Muller, D.J. and Franz, C.M. (2007) Revealing early steps of $\alpha 2\beta 1$ integrin-mediated adhesion to collagen type I by using single-cell force spectroscopy. Mol. Biol. **18**(May), 1634–1644

Tsukasaki, Y., Kitamura, K., Shimizu, K., Iwane, A.H., Takai, Y. and Yanagida, T. (2007) Role of multiple bonds between the single cell adhesion molecules, nectin and cadherin, revealed by high sensitive force measurements. J. Mol. Biol. **367**(**4**), 996–1006

Veneziano, R., Rossi, C., Chenal, A., Devoisselle, J.-M., Ladant, D. and Chopineau, J. (2013) Bordetella pertussis adenylate cyclase toxin translocation across a tethered lipid bilayer. Proc. Nat. Acad. Sci. U.S.A. **110**(**51**), 20473–20478

Vojtova, J., Kamanova, J. and Sebo, P. (2006) Bordetella adenylate cyclase toxin: a swift saboteur of host defense. Curr. Opin. Microbiol. **9**, 69–75

Williams, P.M. (2003) Analytical descriptions of dynamic force spectroscopy: behaviour of multiple connections. Anal. Chim. Acta **479**(**1**), 107–115

Yaghi, A. and Dolovich, M. (2016) Airway epithelial cell cilia and obstructive lung disease. Cells **40**(**5**), 1–19

Zhang, X., Chen, A., De Leon, D., Li, H., Noiri, E., Moy, V.T. and Goligorsky, M.S. (2004) Atomic force microscopy measurement of leukocyte-endothelial interaction. Am. J. Physiol. Heart Circ. Physiol. **286**(**1**), H359–H367

Received: 20 December 2016; Revised: 1 June 2017; Accepted: 2 June 2017; Accepted article online: 9 June 2017

